JOURNAL OF MATERIALS SCIENCE 22 (1987) 737–744

Laser-induced vapour-phase syntheses of boron and titanium diboride powders

J. DAVID CASEY, JOHN S. HAGGERTY
Energy Laboratory, Massachusetts Institute of Technology, Cambridge, Massachusetts 02139, USA

Small diameter boron and titanium diboride powders were synthesized from vapour phase reactants heated with infrared radiation from a CO_2 laser. Boron powders were synthesized from $BCl_3 + H_2$ gas mixtures and from B_2H_6. $TiCl_4 + B_2H_6$ gas mixtures yielded TiB_2 powder. $BCl_3 + H_2 + TiCl_4$ gas mixtures yielded $TiCl_3$ powder but no TiB_2. Novel equipment designed to vapourize $TiCl_4$ liquid is described. Detailed characterizations of the product powders are presented.

1. Introduction

Silicon, Si_3N_4 and SiC powders have previously been synthesized by heating gases with the infrared radiation (IR) from a CO_2 laser [1–4]. These procedures take advantage of the strong absorptivity of silane (SiH_4) gas at 10.59 μm, the dominant wavelength of an untuned CO_2 laser. The laser-induced vapour-phase process has successfully produced silicon-based powders with a superior morphology. These powders are free of aggregates and composed of small spheres having a narrow size distribution. Recently laser-synthesized silicon powders have been used to make reaction bonded Si_3N_4 pellets with superior microstructures and physical properties [5].

Here we extend the laser-induced vapour-phase process to the production of boron and titanium diboride powders.

Boron powders, with a morphology similar to the laser-synthesized silicon-based powders, are required to fabricate boron containment structures for nuclear reactors. Additionally, we are interested in the characteristics of laser-synthesized boron powders because of our continuing effort to dope SiC powders during the laser-synthesis process with boron, which acts as a sintering aid. The study of the boron laser-chemistry may also increase our understanding of boron doping in hydrogenated silicon films made for semiconductor applications [6] by laser-induced chemical vapour deposition.

Titanium diboride has thermal and electrical conductivities and high resistance to corrosion in molten metals which make it an attractive candidate for cathodes and containers in aluminium reduction cells. The elimination of microstructural defects, a source of corrosion failure in TiB_2 pieces, requires TiB_2 powders with superior properties similar to the laser-synthesized silicon-based powders described above.

In this study, boron trichloride (BCl_3) and diborane (B_2H_6) were used as boron sources and titanium tetrachloride ($TiCl_4$) as the titanium source in the laser-syntheses. BCl_3 and B_2H_6 also served as the infrared radiation absorbers in their respective reaction mixtures. Achieving these laser-induced reactions presented several new experimental problems including a reactant ($TiCl_4$) which is liquid at ambient conditions, corrosive reactants and products, and the endothermicity of the predicted chemical reactions. Methods of addressing these problems are described.

Boron powders are synthesized from $BCl_3 + H_2$ which have different morphologies from the boron powders produced from B_2H_6. We successfully synthesized TiB_2 from $TiCl_4 + B_2H_6$ but were unable to generate TiB_2 powder from $TiCl_4 + BCl_3 + H_2$. Detailed characterizations of the powders are presented.

2. Experimental procedure

The laser powder synthesis cell and synthetic procedures have been described in detail elsewhere [1, 3, 4]. Briefly, a vertical stream of reactant gases enters the stainless steel reaction cell (Fig. 1) from the bottom through a 1.4 mm i.d. stainless steel nozzle and intersects the horizontal 10.591 μm wavelength beam of a 150 W, continuous wave CO_2 laser. The nozzle is set in a removable, stainless steel 1-inch VCR gland (Cajon Co., Macedonia, Ohio) attached with a gasket seal to the bottom of the cell. The beam is focused with gallium arsenide lenses; a 13 cm focal length lense was used for most of the reactions. The laser beam enters and exits the cell through IR-transparent KCl windows and the reaction zone can be observed through fused silica windows. The hot product powders form a bright incandescent plume. A 1.0 litre min^{-1} coaxial stream of argon gas (annular gas) is used to entrain the product powders which are collected at the top of the cell in a cylindrical borosilicate glass resin filter (an A-H type filter, Balston Filter Products, Lexington, Massachusetts). The filter is contained in a stainless steel Balston filter housing unit fitted with ball valves on both ends. After a synthesis experiment, the ball valves are closed and the powder is transferred to an inert-atmosphere glove box without exposure to air. The mass flow rates of the gases are controlled by electronic mass flow controllers or by rotometers. The cell pressure is continuously regulated by a solenoid valve positioned on the downstream side of the filter

0022–2461/87 $03.00 + .12

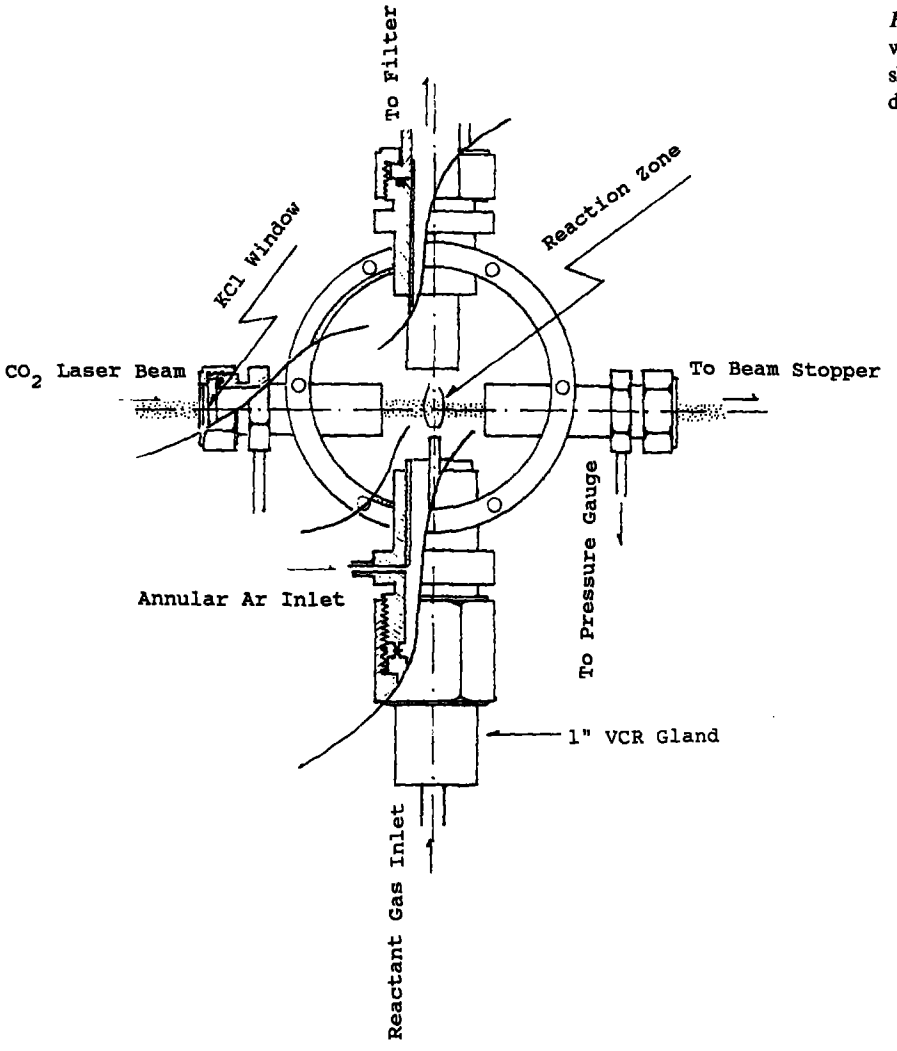

Figure 1 The laser powder synthesis cell without the modified nozzle assembly shown in Fig. 2. See the text for a detailed discussion.

housing unit and governed by a commercial pressure-control unit. The downstream side of the solenoid valve is continually pumped with a rotary oil vacuum pump.

Several modifications to these previously published procedures were required for boron and TiB_2 syntheses. The 1-inch, stainles steel VCR gland shown in Fig. 1 was modified (Fig. 2) to continuously vaporize the $TiCl_4$ liquid; it was machined to receive the liquid reactant in its centre bore and additional gaseous reactants in a diagonal bore. Three 50 W cartridge heaters positioned symmetrically around the centre bore heated the liquid $TiCl_4$. K-type thermocouples, inserted into wells in the walls of the heated nozzle assembly, sensed its temperature and a commercial temperature control unit held the heated nozzle temperature at the desired value. The coaxial argon gas stream was also heated to prevent condensation of the $TiCl_4$ vapour in the synthesis cell.

The liquid $TiCl_4$ was metered into the centre bore of the heated nozzle assembly through a 0.45 mm i.d. stainless steel line attached to a Pressure-Lok Series A-2, gas tight syringe (Dynatech Corp., Baton Rouge, Los Angeles) which was driven by a syringe pump. Before loading the $TiCl_4$ liquid, the stainless steel line and the syringe were evacuated to a pressure below 10 μm Hg for several hours to remove adsorbed water vapour.

An important modification was the substitution of a water-primed ring pump (Model A-1, Atlantic Fluidics, Inc., Stamford, Connecticut) for the rotary oil vacuum pump to continuously pump the reaction cell during powder synthesis experiments. The circulating water neutralized corrosive gases such as unreacted $TiCl_4$ and BCl_3 and reaction byproducts such as HCl. In addition, any unreacted B_2H_6, diluted with the annular argon gas, was hydrolized in the pump to innocuous boron oxide.

The brightness temperature of the reaction zone, the volume in which gaseous reactants were converted to hot powders, was measured with an optical pyrometer. To monitor the stability of the process, a photodiode measured fluctuations in a 5 mW HeNe laser beam (λ = 632.8 nm) that passed through the powder plume. The fraction of the beam transmitted was sensitive to the composition of the reaction zone and fluctuations indicated irregular vaporization of the $TiCl_4$ liquid.

The $TiCl_4$ (Alfa Products, Danvers, Massachusetts) was distilled in an inert atmosphere prior to use. Research grade BCl_3 and H_2 gases and B_2H_6 gas (Callery Chemical Co., Callery, Pennsylvania) were used without further treatment.

The powders were characterized by the following techniques; X-ray diffraction (Cu$K\alpha$), transmission electron microscopy (TEM), single point BET surface area anaylsis, and simultaneous thermal gravimetric and differential thermal analyses (TGA/DTA). Powder

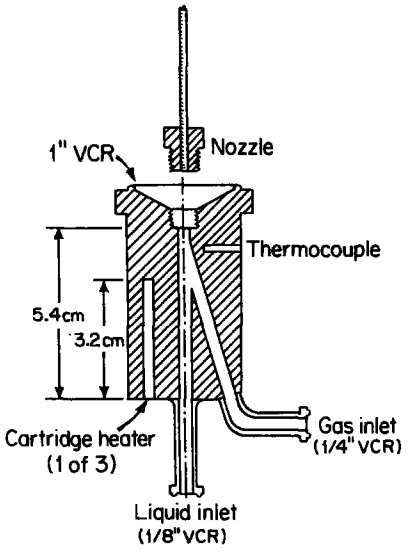

Figure 2 The heated nozzle assembly. See text for a detailed discussion.

samples for electron microscopy were prepared by dipping 100-mesh copper TEM grids into sonicated dispersions of the powder in isopropanol.

Titanium analyses were done by atomic absorption spectroscopy. The boron analyses were done by inductively coupled plasma-emission spectroscopy. Chloride analyses involved combusting the powders in O_2 and dissolving the residue in 2% w/v hydrazine sulphate, acidified with nitric acid; this solution was potentiometrically titrated with silver nitrate. All analyses were done by Galbraith Laboratories, Knoxville, Tennessee.

Equilibrium quantities and compositions of gaseous and condensed species were determined utilizing SOLGASMIX-PV, a thermodynamic analysis program [7, 8] which minimizes the free energy of a chemical system while conserving the total mass of the system. Thermodynamic data were obtained from the Joint Army Navy Air Force (JANAF) computerized thermochemical data base. All SOLGASMIX-PV runs were made at constant pressure conditions.

3. Results and discussion

3.1. Boron trichloride chemistry

The initial experiments on boron and TiB_2 powders utilized BCl_3 as the boron source for several reasons: (1) the absorptivity of BCl_3 [9, 10] is greater than that of B_2H_6 [11] at 10.59 μm; (2) BCl_3 is less dangerous than the toxic and explosive B_2H_6 and (3) BCl_3 is less than 10% as costly as B_2H_6 ($300 per kilogram of BCl_3 [Matheson Gas Products, Gloucester, Massachusetts] against $4700 per kilogram of B_2H_6 [Callery Chemical Co., Callery, Pennsylvania]).

The overall gas-phase reactions, by which boron and TiB_2 were synthesized from BCl_3, are described by the following, balanced equations:

$$BCl_3(g) + 3/2H_2(g) \rightarrow B(s) + 3HCl(g) \quad (1)$$

$$TiCl_4(g) + 2BCl_3(g) + 5H_2(g) \rightarrow TiB_2(s) + 10HCl(g) \quad (2)$$

Since both H_2 and $TiCl_4$ are transparent to 10.59 μm radiation, the infrared radiation is absorbed only by BCl_3 and the absorbed energy is transferred to the other reactant gases by intermolecular collisions [1].

In the 927 to 1427° C range, boron formation from BCl_3 plus H_2 is endothermic [12] by approximately + 117 kJ mol^{-1} with free energies of formation ranging from + 36 kJ mol^{-1} at 927° C to + 1.7 kJ mol^{-1} at 1427° C. Over the same temperature range, the TiB_2 synthesis is endothermic by approximately + 335 kJ mol^{-1} and the free energy of formation varies from + 22.6 kJ mol^{-1} at 927° C to − 107.5 kJ mol^{-1} at 1427° C. In spite of the large positive enthalpies of formation, TiB_2 films have been deposited on hot substrates using gas mixtures of a $TiCl_4$, H_2 and BCl_3 [13, 14] while boron has been generated from gas mixtures of BCl_3 plus H_2 [15].

With only BCl_3 passing through the CO_2 laser beam, we observed a previously reported [16] white luminescent zone, but we detected no powder formation by HeNe light scattering. A brightness optical pyrometer temperature of 1175° C was observed for 15 sccm (standard cubic centimeters per minute) BCl_3, 0.99 × 10^5 Pa cell pressure, with a focused (2 mm diameter, 4.8 × 10^3 W cm^{-2}) infrared beam.

The addition of H_2 gas to the BCl_3 stream resulted in powder formation, observed both visually and by HeNe light scattering. Flow rates of 15 sccm BCl_3 and 25 sccm H_2 at a laser intensity of 4.8 × 10^3 W cm^{-2} yielded a maximum brightness optical pyrometer temperature of 1370 to 1430° C; 10 to 15% of the BCl_3 was converted to boron powder. An equilibrium thermodynamic calculation predicts that approximately 35% of the BCl_3 forms boron powder at 1427° C. Possible explanations for the less-than-theoretical yields are the unusually high gas heating rates (10^5–10^6° C sec^{-1}) and short residence times (10^{-3} sec) in the reaction zone which are characteristic of the laser-induced vapour-phase process. Also some of the gas stream is heated to cooler temperatures because it passes around rather than through the focused laser beam. Measured powder characteristics are reported in Table I. The specific surface area of the powder is smaller than reported for the B_2H_6 reactions and the corresponding equivalent spherical diameter is larger (vide supra). The greyish brown powder is amorphous (X-ray) and contains little, if any, volatile side products (no weight loss during TGA/DTA in argon, 20° to 1225° C). TEM micrographs of the boron powder are shown in Fig. 3. A variety of particle types exist. A few particles as small as 20 to 30 nm in diameter are evident, the majority are non-equiaxed and between 150 and 200 nm (Fig. 3a), and a few particles as large as 1300 nm are present. A small fraction of the particles are perfect spheres with 80 to 100 nm diameters (Fig. 3b). The boron particles are not agglomerated. The particle size range and the most-frequently-observed sizes agree qualitatively with the BET results, indicating little internal porosity in the powders. Electron diffraction patterns are not observed for this as-synthesized boron powder, confirming the X-ray diffraction observation that the boron powder is amorphous.

Even after the boron powder was heated to 1225° C

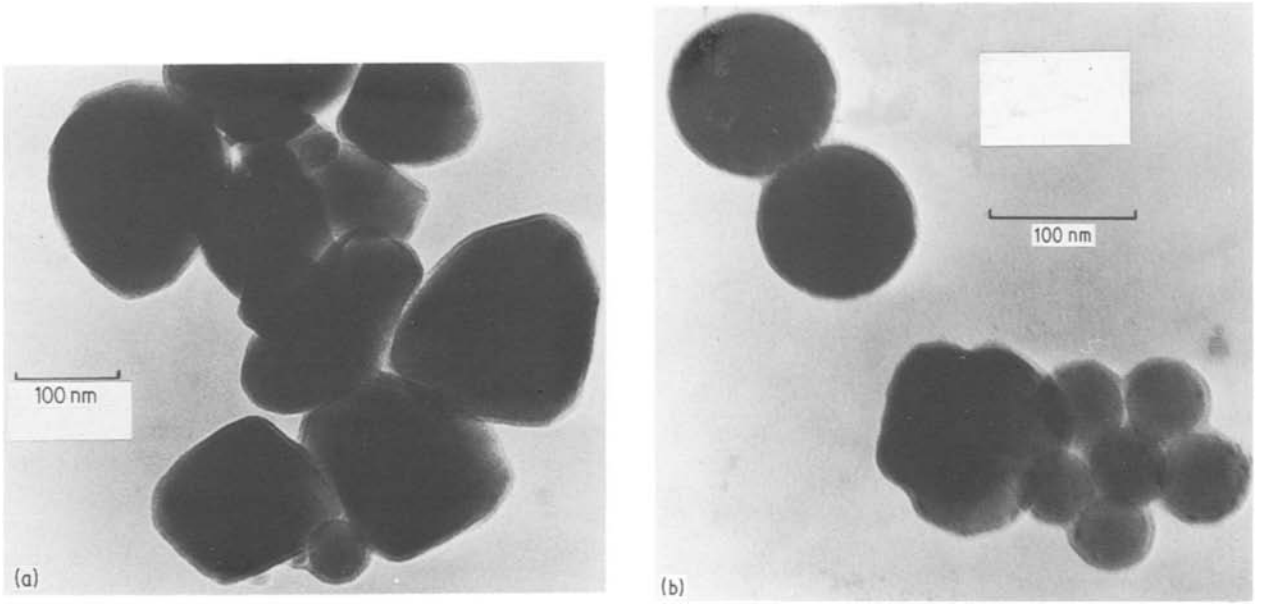

Figure 3 Bright-field transmission electron micrographs of as-synthesized boron powder from $BCl_3 + H_2$ (A-070B powder). (a) Micrograph of typical particles and (b) atypical perfectly spherical particles.

in argon, faint boron X-ray diffraction rings could only be seen following a 7 h exposure to Co$K\alpha$ radiation in a Debye-Sherrer camera; the *d*-spacings of 0.506, 0.440, 0.398, 0.253 and 0.204 nm correspond to reported values for rhombohedral boron [17].

The bright field pictures of this heat-treated boron powder are similar to the as-synthesized powder, but now electron diffraction patterns are observed which correspond to *d*-spacings of 0.417, 0.237 to 0.246, 0.188 to 0.197, 0.166 to 0.173 and 0.136 to 0.145 nm; rhombohedral and tetragonal boron have comparable *d*-spacings [18].

The addition of $TiCl_4$ vapour to the BCl_3 plus H_2 gas stream caused the luminous reaction zone to change from a bright white plume to a cherry red sheath surrounding a bright white centre. HeNe scattering did not detect powder formation in the white central portion of the reaction zone where the CO_2 laser beam and the gas stream intersect. However, powder formation was observed a centimeter downstream from the maximum temperature region in cooler regions of the gas stream. The BCl_3 and $TiCl_4$ mass-flow rates (Table I) were varied in an attempt to produce a normal, stable reaction zone, but powder persisted in forming beyond the maximum temperature region of the gas stream as well as in cooler regions of the reaction cell outside the boundaries of the annular argon stream. The as-produced powder had a purple-brown colour. After air exposure the powder lost its violet colour and turned grey-white. X-ray diffraction analysis (Table I) of the unexposed powders indicated the presence of $TiCl_3$ [19], a violet material with a relatively low boiling point (660° C at 0.144×10^5 Pa). Evidently this compound was generated as a gas in the reaction zone, and condensed to solid particles in cooler regions of the reaction cell. Its presence beyond the annular stream boundaries indicate that the annular argon stream is efficient in entraining solid but not gaseous reaction products.

The formation of $TiCl_3$ from $TiCl_4$ is described by the following equation:

$$TiCl_4(g) + 1/2H_2(g) \rightarrow TiCl_3(g) + HCl(g) \quad (3)$$

The standard free energy of formation [11] of $TiCl_3$

TABLE I Synthesis conditions and powder characteristics of powders from BCl_3 chemistries

Laser intensity ($W\,cm^{-2}$)	Cell pressure (10^5 Pa)	BCl_3 sccm	H_2 sccm	$TiCl_4$ sccm	Brightness reaction zone temperature (° C)	Yield	Powder appearance	Specific[a] surface area ($m^2\,g^{-1}$)	BET equivalent spherical diameter (nm)	X-ray diffraction
2×10^4	0.99	15	25	–	1370–1430	10–15%	Greyish brown	19.4	130.8[b]	No peaks
4.8×10^3	~0.88	10–50	25	6–30	1100 at 19 sccm $TiCl_4$ and 10 sccm BCl_3	Not determined	Purple brown	9.2	[c]	$TiCl_3$[d]

[a]Powders were outgassed in BET cell for 2 h at 200° C under N_2 gas flow before making BET gas desorption measurements.
[b]Equivalent spherical diameter for boron was calculated from BET surface area by using 2.37 $g\,cm^{-3}$ for the boron density in the equation, $d = 6s^{-1}\varrho^{-1}$ in which *d* is the equivalent spherical diameter, *s* is the surface area and ϱ is the powder density.
[c]Equivalent spherical diameter was not calculated from the BET surface area because the powder density, which depends on the exact chemical composition of the product powder, is not known.
[d]The X-ray diffraction of the violet powder had peaks at corresponding to *d*-spacings of 0.2763 and 0.1790 nm with peak line widths corresponding to crystallite sizes of 42.5 and 157.5 nm respectively.

TABLE II Synthesis conditions and powder characteristics of boron powder from B_2H_6 chemistry

Run number	Laser intensity ($W cm^{-2}$)	Cell pressure (10^5 Pa)	B_2H_6 sccm	H_2 sccm	Brightness reaction zone temperature (° C)	Yield	Specific[a] surface area ($m^2 g^{-1}$) BET	BET equivalent spherical diameter[b] (nm)	X-ray diffraction
A-052B	2×10^4	0.64	6	6	1160–1170	38%	46.2	54.8	amorphous
A-043B	2×10^4	0.71	10	–	1380	Not determined	62.2	41.0	amorphous[c]
A-050B	2×10^4	0.67	12	12	1290–1300	62%	52.3	48.3	amorphous
A-068B	2×10^4	0.99	12	–	1350–1380	54%	56.0	45.2	amorphous
A-044B	2×10^4	0.71	25	–	1495	Not determined	72.0	35.6	amorphous[c]
A-071B	2×10^4	0.99	36	–	1460–1470	83%	72.6	34.9	amorphous

[a] Powders were outgassed in BET cell at 200° C for 2 h with N_2 gas flow before making BET gas desorption measurements.
[b] Equivalent spherical diameter for boron was calculated from BET surface area by using 2.37 $g cm^{-3}$ for boron density in the equation, $d = 6s^{-1}\varrho^{-1}$ in which d is the equivalent spherical diameter, s is the surface area and ϱ is the powder density.
[c] Following a 20 to 1500° C heat treatment in argon gas, A-043B powder had a boron diffraction pattern. Crystallite sizes of 28.7 and 42.4 nm were determined for lines corresponding to 0.411 and 0.258 nm d-spacings, respectively. After the same heat treatment, A-044B powder had a boron diffraction pattern with crystallite sizes of 34.1 and 28.1 nm determined at the same 2θ positions, respectively.

varies from $+34.3$ kJ mol^{-1} at 927° C to -0.4 kJ mol^{-1} at 1427° C while the enthalpy remains constant at approximately $+125$ kJ mol^{-1}. Once the infrared energy has been absorbed by BCl_3, the energy is rapidly transferred to the other reactant molecules, producing a uniformly hot reaction zone in which $TiCl_3$ formation [20, 21] can compete with TiB_2 formation.

We conclude that the BCl_3 plus H_2 reactants produce laser-synthesized boron powders with interesting morphologies and that further study would be advantageous. The laser-synthesis of TiB_2 powder from BCl_3, H_2 and $TiCl_4$ is less promising. The large endothermic heat of reaction (335 kJ mol^{-1}) and competing reaction pathways are difficult obstacles for the laser-synthesis process to overcome.

3.2. Diborane chemistry

Although our operating laser wavelength, 10.59 μm, was not ideal for B_2H_6 absorption [11], we were able to synthesize both boron and TiB_2 powders using the laser-induced vapour-phase method with B_2H_6 as the boron source. Previously, boron [22, 23] and TiB_2 [24, 25] films had been formed by reactions involving thermal decomposition of B_2H_6.

3.2.1. Boron synthesis

The formation of boron powder from B_2H_6 is thermodynamically favoured. The reaction $B_2H_6 \rightarrow 2B + 3H_2$ is exothermic [12] by -22.8 kJ mol^{-1} with a -272 kJ mol^{-1} free energy of formation at 927° C; the enthalpy and free energy are -25 and -375 kJ mol^{-1}, respectively, at 1427° C.

When utilizing an unfocused (6 mm diameter, 530 $W cm^{-2}$) CO_2 laser beam, powder formation could be detected by HeNe light scattering as the B_2H_6 flow rate was increased above 12 sccm (at 0.71×10^5 Pa cell pressure), but visible luminescence was never observed. However, as the laser beam was focused, the reaction zone ignited, that is, powder formation was accompanied by bright visible luminescence. The boron syntheses were done with a focused beam diameter of 1 mm (2×10^4 $W cm^{-2}$).

Some boron synthesis conditions and powder characteristics are listed in Table II. All the boron powders were greyish brown. Increasing the B_2H_6 mass flow rates increased the reaction zone temperature while H_2 addition to the reactant stream caused a temperature drop (e.g. A-050B against A-068B and A-043B). Hotter reaction zone temperatures (A-071B against A-068B) produced higher product yields and powders with higher specific surface areas and correspondingly smaller equivalent spherical diameters. The as-synthesized powders were amorphous, but boron crystallites were detected by X-ray diffraction [18] following TGA/DTA in argon to 1500° C (A-043B and A-044B) in which no weight change was observed. A 15 to 40 nm crystallite size range was determined by X-ray line width analysis of the lines for the 0.4114 and 0.2578 nm d-spacings. Following heating in air to 400° C, the X-ray diffraction of A-068B indicated crystalline B_2O_3 [26] in the boron powder; higher temperatures produced an amorphous B_2O_3 melt (460° C melting point). Hydrogen addition to the B_2H_6 reactant did not noticeably affect the powder characteristics.

Chemical analyses of as-synthesized A-071B and A-068B powders detected 96.8 and 96.3 wt % boron, respectively; a reference sample of commercial boron (Callery Chemical Co, Callery, Pennsylvania) was 96.2 wt % boron.

TEM micrographs of as-synthesized powders (Fig. 4) showed approximately spherical, non-textured boron particles with 30 to 40 nm diameters arrayed in chains and small clusters. A few larger ($\sim$280 nm) particles were observed. These observations agree qualitatively with BET equivalent spherical diameters, indicating the absence of internal porisity in the powders. Electron diffraction patterns were not observed with the as-synthesized boron powders.

The boron contents of the powders formed from B_2H_6 are high, but the powder morphologies are not ideal. The boron powder formations are similar to those of the laser-synthesized silicon powders produced at low reaction-zone temperatures (1100 to 1300° C). Very noticeable improvements in the silicon morphologies were made by raising the temperature of the silicon reaction zone above 1400° C, the silicon melting point. Larger, spherical, non-agglomerated

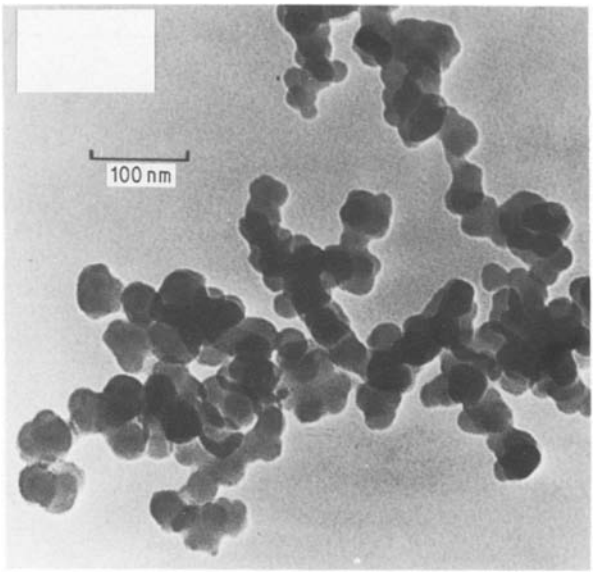

Figure 4 Bright field transmission electron micrograph of the as-synthesized powder from B_2H_6. (A-071B powder.)

powders were obtained. Testing this approach on boron powder synthesized from B_2H_6 would require a larger CO_2 laser to raise the reaction temperature above 2250° C, the boron melting point.

3.2.2. Titanium diboride synthesis

The addition of $TiCl_4$ vapour into the B_2H_6 gas stream increased the brightness optical pyrometer temperatures in the reaction zone and decreased the intensity of the HeNe laser beam transmitted through the powder plume. These two parameters were used to monitor the reproducibility and the stability of the $TiCl_4$ vaporization process, which was the most difficult parameter to control. The most favourable operating conditions for uniform $TiCl_4$ vaporization were cell pressures of 0.80 to 0.99 $\times$ 10^5 Pa and a heated nozzle temperature of approximately 120° C. These conditions approximate an equilibrium liquid–vapour state of $TiCl_4$ (boiling point of 136° C at 1.01 $\times$ 10^5 Pa).

Table III lists synthesis conditions and powder characteristics for TiB_2 powder; some experiments had H_2 added to the $TiCl_4 + B_2H_6$ reactant mixture. A focused CO_2 laser beam (1 mm diameter, 2 $\times$ 10^4 W cm^{-2}) was used at all times. When maintaining stoichiometric mass flow rates ($1TiCl_4 : 1B_2H_6$ ratio), higher total mass flows showed higher optical pyrometer temperatures and had powder plumes which were less transparent to the HeNe beam. The addition of H_2 gas lowered the optical pyrometer temperature slightly (A-048TB against A-051TB and A-045TB against A-053TB), while at specific B_2H_6 mass flow rates, increased $TiCl_4$ flow caused higher optical pyrometer temperatures (A-045TB and A-047TB against A-054TB and A-055TB). Increased cell pressures also caused minor temperature elevations (A-058TB against A-048TB).

The product powders were black and had a pungent odour. The powders were extremely pyrophoric, burning vigorously when exposed to air. After burning, the resulting white powder exhibited both $TiBO_3$ [27] and B_2O_3 [26] X-ray diffraction patterns.

The as-synthesized black powders have 30–50 $m^2 g^{-1}$ specific surface areas with a corresponding 30 to 50 nm equivalent spherical diameters. They exhibited TiB_2 X-ray diffraction patterns [27]; the most intense peaks usually are the 1 0 0 plane (0.263 nm *d*-spacing), the 1 0 1 plane (0.204 nm *d*-spacing) and 0 0 1 plane (0.323 nm *d*-spacing). A TiB_2 crystallite size range of 9 to 30 nm was determined from these X-ray line widths. TEM micrographs (Fig. 5) show a variety of particle shapes and sizes, 20 to 30 nm faceted particles, 20 to 100 nm polycrystalline particles and occasionally particles larger than 100 nm. Dark field TEM microscopy of the as-synthesized powder showed that the powders were polycrystalline and were composed of

TABLE III Synthesis conditions and powder characteristics of TiB_2 powder from B_2H_6 chemistry

Run number	Laser intensity ($W cm^{-2}$)	Cell pressure (10^5 Pa)	$TiCl_4$ sccm	B_2H_6 sccm	H_2 sccm	Brightness reaction zone temperature (° C)	Specific surface area ($m^2 g^{-1}$) BET[a]	BET equivalent spherical diameter[b] (nm)	X-ray diffraction	TiB_2 crystallite[c] size (nm)
A-066TB	2 $\times$ 10^4	0.99	8	8	–	1460–90	32.0, 47.8	47.9, 32.1	TiB_2	12–18
A-058TB	2 $\times$ 10^4	0.83	12	12	–	1510–30	45.2	33.9	TiB_2	12–14
A-057TB	2 $\times$ 10^4	0.83	12	12	–	1510–35	51.4		TiB_2	12–13
A-056TB	2 $\times$ 10^4	0.72–0.83	12	10	–	1490–1530	52.3		TiB_2	100–29
A-048TB	2 $\times$ 10^4	0.67	12	12	–	1460–75	35.4		TiB_2	8–9
A-051TB	2 $\times$ 10^4	0.80	12	12	12	1420–50	48.4		TiB_2	8–20
A-055TB	2 $\times$ 10^4	0.83	12	6	–	1470	41.7		TiB_2, $TiCl_3$[d]	10–13
A-054TB	2 $\times$ 10^4	0.71–0.73	8	6	–	1470–90	30.1		TiB_2	10–30
A-047TB	2 $\times$ 10^4	0.64	6	6	–	1360–80	31.8		TiB_2	8–10
A-045TB	2 $\times$ 10^4	0.64–0.71	6	6	–	1370–80	48.5		TiB_2	8–22
A-053TB	2 $\times$ 10^4	0.64	6	6	6	1330–40	34.2		TiB_2	9–20

[a] Powders were outgassed in BET cell for 2 h at 200° C under N_2 gas flow before making BET gas desorption measurements.

[b] BET equivalent spherical diameters of these powders are calculated from BET surface areas by using weighted values for the powder density in the equation, $d = 6s^{-1}\varrho^{-1}$ in which d is the equivalent spherical diameter, s is the surface area and ϱ powder density. The weighted density value is calculated by assuming TiB_2 and boron are the only solid products. Using this assumption, the chemical composition of A-066TB converts to $2.63TiB_2 : 1.0B$ and A-058TB converts to $2.67\ TiB_2 : 1.0B$. Since chemical analyses were not done on the other powders, weighted density values could not be calculated.

[c] The TiB_2 crystallite size range was determined from the widths of the X-ray lines corresponding to 0.263, 0.204 and 0.323 nm *d*-spacings.

[d] Diffraction peaks indicated the presence of γ-$TiCl_3$ [19].

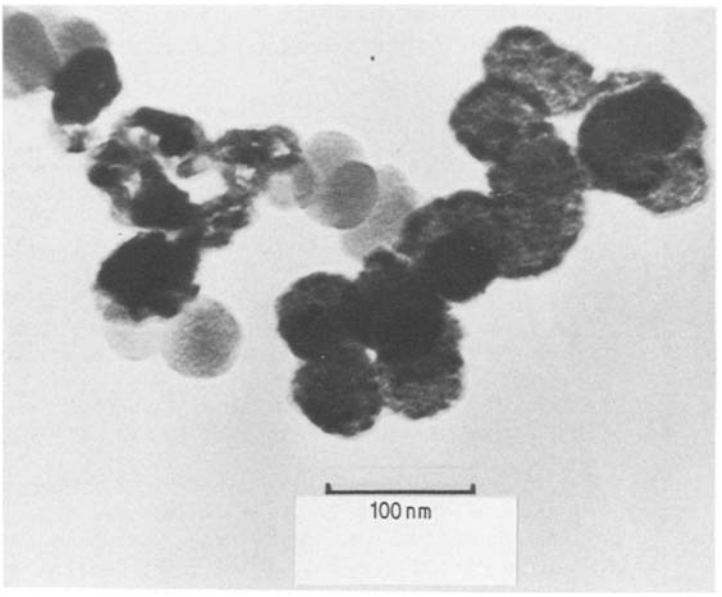

Figure 5 Bright field transmission electron micrographs of the as-synthesized powder from $TiCl_4 + B_2H_6$. (A-057TB powder.)

nominally 10 nm crystallites which closely match the values calculated by X-ray line width analysis. The electron diffraction patterns closely matched those of commercial TiB_2 powder (Gallard-Schlesinger Chemical Mfg., Corp.). Some other particle types are present in Fig. 5 which showed low contrast in both absorption and diffraction of the electron beam. These particles were most likely boron, being very similar to the boron particles which were synthesized from B_2H_6 (Fig. 4).

Frequently the black product powders had traces of violet material; this was most evident in experiment A-055TB in which excess $TiCl_4$ was used in the reactant mixture. X-ray diffraction analysis detected the presence of γ-$TiCl_3$ [19], a violet solid, in addition to TiB_2. As previously discussed for $TiCl_4$, BCl_3, H_2 reactant mixture, $TiCl_3$ formation also competes with the TiB_2 pathway in the $TiCl_4$, B_2H_6 system [24]. Advantages of B_2H_6 over BCl_3 are that boron is not initially bound to chlorine in a stable molecule and that less total chlorine is available to influence the final end product composition.

A-066TB and A-058TB powders were chemically analysed. These syntheses had especially uniform and controlled vaporizations of the $TiCl_4$ liquid during the entire experiment. The elemental mole ratio B : Ti : Cl was 2.38 : 1.00 : 0.20 for A-066TB and 2.37 : 1.00 : 0.34 for A-058TB; while a reference sample of commercial TiB_2 was 1.87B : 1.00Ti : 0.0Cl. The excess boron in the laser-synthesized TiB_2 powders is, at least partially, explained by our procedure of initiating a synthesis experiment by first flowing and igniting the B_2H_6 gas before introducing $TiCl_4$ vapour and of terminating an experiment by first stopping the $TiCl_4$ flow.

For a $1TiCl_4 : 1B_2H_6$ gas mixture, SOLGASMIX-PV calculations, which were insensitive to 0.27 to 0.93×10^5 Pa pressure variations, predicted TiB_2 yields of 66, 80 and 89% at 530, 1230 and 1330° C, respectively. Our experimental TiB_2 yields were 50 to 70% with 1460 to 1530° C reaction zone temperatures (A-066TB and A-058TB). As previously discussed, inherent characteristics of the laser-synthesis process possibly explain the fact that TiB_2 yields are less than predicted; for example, the very high reactant heating rates, the short residence times in the reaction zone and the fact that some of the reactant gas stream may be heated to cooler temperatures because it passes around, rather than through, the focused laser beam.

Additional predicted equilibrium species were $TiCl_4$, $TiCl_3$ and BCl_3 with molar compositions of $2TiB_2 : 1TiCl_4 : 0TiCl_3 : 2BCl_3$ at 530° C, $11.4TiB_2 : 1.9TiCl_4 : 1TiCl_3 : 4.8BCl_3$ at 1230° C and $17.8TiB_2 : 1.2TiCl_4 : 1TiCl_3 : 3.8BCl_3$ at 1330° C. Elevated reaction temperatures improved the calculated yields of TiB_2 and increased the $TiCl_3$ content. Boron formation was not predicted by SOLGASMIX-PV calculations. Because the powders were degassed under vacuum in the powder collection chamber following syntheses, any residual $TiCl_4$ or BCl_3 would not be retained in the powder and therefore not detected by chemical analyses.

The powders were heated in the TGA/DTA apparatus under argon at a heating rate of $5° C min^{-1}$. Endothermic weight losses of 6 to 9% were observed at 100 to 150° C and at 600 to 700° C. Before argon heat treatment the BET surface area of A-066TB powder was $32.0 m^2 g^{-1}$, but decreased to $18.6 m^2 g^{-1}$ after heating to 700° C and to $1.4 m^2 g^{-1}$ after heating to 1500° C. The X-ray diffraction line widths of this TiB_2 powder were also affected by the elevated temperatures. Before heat treatment a 12.5 to 18.0 nm crystallite size was determined for A-066TB powder; heating to 700° C did not have much effect but the crystallite size was increased to 55 to 69 nm after heating to 1500° C. Dark field TEM microscopy of the TiB_2 heated to 1500° C showed that enlarged, faceted crystallites with 70 to 160 nm dimensions (Fig. 6) have replaced the polycrystalline particles observed after synthesis (Fig. 5).

4. Conclusions

We have successfully modified the laser-induced vapour-phase synthesis process to include endothermic reactions involving corrosive species and liquid

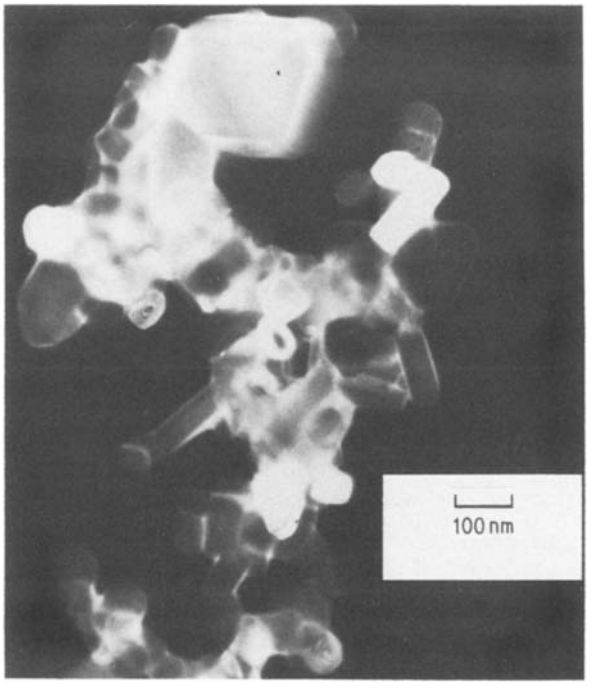

Figure 6 Dark field transmission electron micrograph of TiB_2 powder following heat treatment in argon to 1500° C. (A-066TB powder.)

reactants. Non-agglomerated, 100 to 200 nm boron powders were synthesized from $BCl_3 + H_2$, but the endothermic barrier for the formation of TiB_2 from $TiCl_4 + BCl_3 + H_2$ was too great for the laser process. The exothermic formation of boron powder from B_2H_6 produced powders with non-ideal morphologies which we anticipate would be improved by increasing the reaction zone temperature. The fine TiB_2 powders formed from $TiCl_4 + B_2H_6$ are polycrystalline and have highly reactive surfaces. Further work on improving the synthetic yields of TiB_2, on modifying the powder morphology and on processing the TiB_2 powders is being contemplated.

Acknowledgements

The authors gratefully acknowledge the assistance of Christopher Harris in powder synthesis; John Flint, Richard Fenner, Robert Cuikay, David Volfson and Carlo Golino in equipment design and assembly; David Ming and Raymond Henry in SOLGASMIX-PV modifications and utilization; Jonathan Suber, Rhonda Fullerton and Sheree Tieh in powder characterization; Howard Branz, Barbara Layne and Cindy Cali in manuscript preparation. Professor Karl E. Spear, from the Pennsylvania State University, is gratefully acknowledged for providing a copy of SOLGASMIX-PV. This work was supported by the Consortium for Processing of Ceramic Powders by Laser Induced Reactions and US Department of Energy (DOE) Grant No. DE-FG07-83ID12380. However, any opinions, findings, conclusions, or recommendations expressed herein are those of the authors and do not necessarily reflect the views of DOE.

References

1. W. R. CANNON, S. C. DANFORTH, J. H. FLINT, J. S. HAGGERTY and R. A. MARRA, *J. Amer. Ceram. Soc.* **65** (7) (1982) 324.
2. W. R. CANNON, S. C. DANFORTH, J. S. HAGGERTY and R. A. MARRA, *ibid.* **65** (7) (1982) 330.
3. J. H. FLINT and J. S. HAGGERTY, SPIE Vol. 458 "Applications of Lasers to Industrial Chemistry" (International Society for Optical Engineering, Bellingham, 1984) p. 108.
4. Y. SUYAMA, R. M. MARRA, J. S. HAGGERTY and H. K. BOWEN, *Amer. Ceram. Soc. Bull.* **64** (10) (1985) 1356.
5. J. S. HAGGERTY, G. GARVEY, J-M. LIHRMANN and J. E. RITTER, "Processing and Properties of Reaction Bonded Silicon Nitride Made from Laser Synthesized Silicon Powders", Symposia L, Defect Properties and Processing of High-Technology Nonmetallic Materials, Materials Research Society Fall Meeting, Boston, Massachusetts (North-Holland, New York, 1985).
6. H. M. BRANZ, S. FAN, J. H. FLINT, B. T. FISKE, D. ADLER and J. S. HAGGERTY, *Appl. Phys. Lett.* **48** (2) (1986) 171.
7. G. ERIKSSON, *Chemica Scripta* **8** (1975) 100.
8. T. M. BESMANN, Report ORNL/TM-5775, Oak Ridge National Laboratory, Oak Ridge, Tennessee 37830 (1977).
9. R. E. SCRUBY, J. R. LACKER and J. D. PARK, *J. Chem. Phys.* **19** (1951) 386.
10. P. L. HOUSTON, A. V. NOWAK and J. I. STEINFELD, *J. Chem. Phys.* **58** (8) (1973) 3373.
11. W. C. PRICE. *J. Chem. Phys.* **16** (9) (1948) 894.
12. "JANAF Thermochemical Tables", Second Edition (Office of Standard Reference Data, National Bureau of Standards, Washington, DC 20234, 1970).
13. H. O. PIERSON and E. RANDICH, *Thin Solid Films* **54** (1978) 119.
14. S. MOTOJIMA, M. YAMADA and U. SUGIZAMA, *J. Nucl. Mater.* **105** (1982) 335.
15. V. I. MATKOVICH (ed.) "Boron and Refractory Borides" (Springer, New York, 1977) p. 219.
16. S. D. ROCKWOOD and J. W. HUDSON, *Chem. Phys. Lett.* **34** (3) (1975) 542.
17. "X-ray Powder Data File", (American Society for Testing and Materials, Philadelphia, Pennsylvania) Data Cards 12-377 and 11-618.
18. *Ibid.*, Data Cards 12-377, 11-618 and 11-617.
19. *Ibid.*, Data Cards 18-1397 and 18-1396.
20. T. M. BESMANN and K. E. SPEAR, *J. Electrochem. Soc.* **124** (5) (1977) 786.
21. H. O. PIERSON and E. RANDICH, *Thin Solid Films* **54** (1978) 119.
22. H. O. PIERSON and A. W. MULLENDORE, *ibid.* **63** (1979) 257.
23. *Idem, ibid.* **83** (1981) 87.
24. *Idem, ibid.* **72** (1980) 511.
25. *Idem, ibid.* **95** (1982) 99.
26. "X-ray Powder Data File" (American Society for Testing and Materials, Philadelphia, Pennsylvania) Data Card 6-0297.
27. *Ibid.*, Data Card 17-310.
28. *Ibid.*, Data Card 8-121.

Received 4 April
and accepted 30 June 1986